

Surfactant-controlled damage evolution during chemical mechanical planarization of nanoporous films

Taek-Soo Kim^a, Tomohisa Konno^b, Reinhold H. Dauskardt^{c,*}

^a Department of Mechanical Engineering, Stanford University, CA 94305, USA

^b JSR Micro, Inc., Sunnyvale, CA 94089, USA

^c Department of Materials Science and Engineering, Stanford University, 496 Lomita Mall, Durand Bldg. Rm. 121, Stanford, CA 94305, USA

Received 12 May 2009; received in revised form 12 June 2009; accepted 16 June 2009

Available online 22 July 2009

Abstract

The integration of nanoporous organosilicate thin films involving chemical mechanical planarization (CMP) is a significant challenge due to the evolution of defects in the films during CMP in the form of cracking and delamination. This study shows that small changes in CMP electrolyte chemistry and surfactant additions can have dramatic effects on crack growth rates in the films. Crack growth rates were sensitive to the type of electrolyte and decreased in the presence of electrolytes that caused crack tip blunting. Growth rates were also sensitive to nonionic surfactant additions where molecular structure and weight were demonstrated to be important variables. An optimized blend of surfactants and electrolytes can significantly retard defect evolution due to molecular bridging. Surfactant self-assembly and resulting molecular bridging were characterized by in situ atomic force microscopy and used to quantify the molecular bridging observed.

© 2009 Acta Materialia Inc. Published by Elsevier Ltd. All rights reserved.

Keywords: Thin films; Nanoporous material; Fracture; Self-assembly

1. Introduction

Processing of thin-film device structures for emerging technologies often involves exposing the structures to moist or chemically active aqueous process environments. The most prominent examples are chemical mechanical planarization (CMP) and post-CMP cleaning, which have become ubiquitous in the processing of Cu interconnects in micro-electronic devices [1]. CMP is designed for precise material removal with extremely high planarity through the mechanically abrasive action of a rotating polishing pad in the presence of slurries containing abrasive particles. This exposes the device structure to normal and shear stresses in the presence of the chemically active aqueous slurry.

The nanoporous organosilicate films used as interlayer dielectrics in interconnect structures are mechanically fragile and susceptible to moisture-assisted cracking, and this leads to damage in the form of fracture and delamination during CMP that has significantly limited the use of these films [2–5]. Similar challenges exist for other emerging applications of nanoporous films including those used for size-selective membranes [6], biosensors [7], optical waveguides [8,9] and photovoltaic cells [10].

Damage evolution during CMP involves the synergistic effects of both process stress and chemistry, although damage has mostly been attributed to the effects of CMP stress [11–13]. Stresses arise not only from the abrasive contact with the rotating CMP pad but also from the inherent film stresses that arise from thermal expansion mismatch and film growth processes. While the effects of stress on fracture processes are well understood, it is not always appreciated that the chemistry of the process or service environments

* Corresponding author. Tel.: +1 650 725 0679; fax: +1 650 725 4034.
E-mail address: dauskardt@stanford.edu (R.H. Dauskardt).

can greatly affect crack growth in thin-film structures. Even small changes in CMP slurry or post-CMP cleaning solution chemistry are known to have dramatic effects on resulting damage [2–4,14,15].

It is well known that increasing humidity or aqueous solution pH greatly accelerates crack growth rates in bulk glasses [16–19] and in organosilicate thin films [2–4,20,21]. In the case of nanoporous glass films, the effects of environment on fracture can be even more complex since diffusion of the environmental species into the nanopores, which is strongly dependent on pH and the presence of organic buffering agents, can lead to a change in the film stress and then even greater effects on cracking [4,22]. Such complex interactions involving solution chemistry and pH have immediate implications for the evolution of CMP damage in nanoporous films when exposed to chemically active slurries. However, given the fragile nature of nanoporous films and their susceptibility to chemically accelerated cracking, it is remarkable that the effects of other essential components of CMP slurries such as alkali metal ions and surfactants have never been studied.

Nonionic surfactants are added to CMP slurries to stabilize particulate dispersions and control the material removal rate. Surfactants improve the contact area between the film surface and the slurry and affect the removal rate by modifying the surface interaction, charge status and polarity of the abrasive [23]. They also enhance the topographical selectivity of barrier layers which are indispensable for uniformity and planarity when two or more materials are polished simultaneously [24]. However, their role on the growth of damage in nanoporous films is currently unknown.

In this study we demonstrate that surfactants in aqueous solutions can significantly affect the crack growth rate in nanoporous organosilicate thin films. This involves the transport of surfactant molecules from the test environment into the nanoscale confined crack and their subsequent interaction with the crack surfaces. These molecular interactions include hydrophilic interactions between the hydrophilic groups on the surfactant molecule and hydroxide terminal groups on the crack surfaces, and hydrophobic interactions between the hydrocarbon chain of the surfactant and methyl groups on the crack surfaces, as schematically illustrated in Fig. 1a. We demonstrate that even small changes in the lengths of either the hydrophobic or hydrophilic groups together with the molecular structure of the surfactants can have dramatic effects on the growth rate of cracks. The suppression of crack growth rates is described in terms of bridging of the crack surfaces by surfactant molecules or the formation of nanobubbles in the surfactant-containing solution. Alternatively, the acceleration of crack growth rates observed for dimeric surfactants are explained in terms of their effect on decreasing the surface energy of the fracture surfaces. The study suggests the potential role of tailoring surfactant additions as crack-inhibiting agents for optimized CMP slurries.

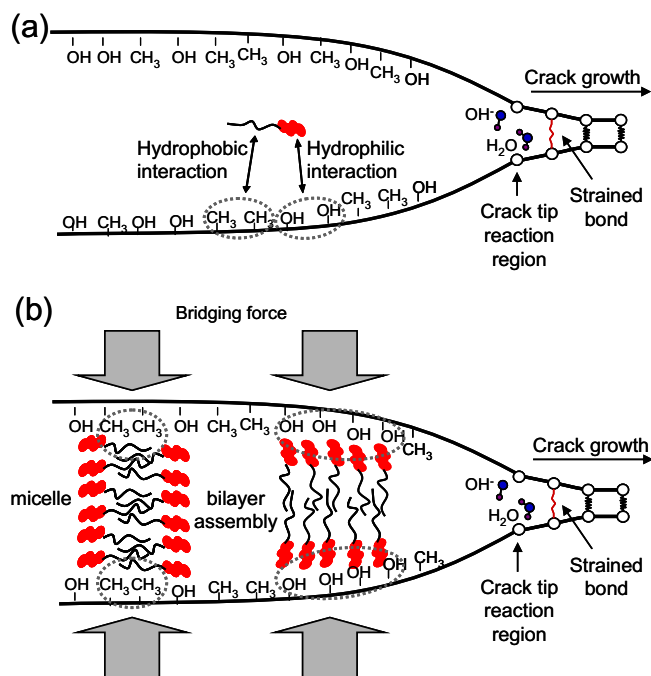


Fig. 1. Schematic illustration of (a) the interaction of a nonionic surfactant molecule with the organosilicate crack surfaces, and (b) two possible surfactant micelle–bilayer bridging assemblies between the crack surfaces.

2. Materials and methods

Double cantilever beam (DCB) specimens were fabricated for crack-growth testing by sandwiching a multilayer thin-film stack between two elastic silicon substrates using previously reported techniques [25,26]. The thin-film stack includes a nanoporous methylsilsesquioxane (MSSQ) film typically used for ultra-low dielectric constant (k) insulating layers. The nanoporous organosilicate film thickness was 500 nm and had a density $\rho \sim 1.06 \text{ g cm}^{-3}$ and pore diameter $d \sim 2.1 \text{ nm}$ measured by positron annihilation lifetime spectroscopy, and a dielectric constant $k \sim 2.3$. The MSSQ glass matrix is a structurally modified form of silica produced by replacing a bridging oxygen atom with a terminal methyl group, yielding a film with reduced k and strong hydrophobicity.

Cracks were introduced in the nanoporous organosilicate film using a pre-notch in the DCB specimen and loading until fracture initiated. The DCB test configuration typically produces cohesive fracture in the center of the brittle nanoporous organosilicate layer, and this was observed for all tests conducted here. Crack growth rates, v , were characterized as a function of the applied strain energy release rate, G , over the range 10^{-4} – $10^{-10} \text{ m s}^{-1}$ using load relaxation fracture mechanics techniques [26]. This involved loading the specimen at a constant displacement rate to a predetermined load, then fixing the displacement. The ensuing time-dependent load relaxation resulting from crack growth increases the specimen compli-

ance from which the crack length, a , v , and G can be calculated. The mean load drift per minute of the load cell was ± 1 mN and this introduced errors in the crack length calculated using compliance techniques and resulting crack growth rate values of $\pm 5 \times 10^{-12}$ m s $^{-1}$ for the low v region ($< 10^{-8}$ m s $^{-1}$). The load drift also caused errors in the calculated G by ± 10 mJ m $^{-2}$. These errors, however, are relatively small and not visible on the scales of the v – G plots. Each v – G curve includes a number of experimental data sets from different specimens, demonstrating significant reproducibility.

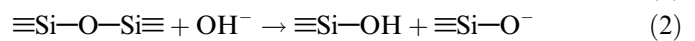
Testing was conducted in an environmental chamber with controlled aqueous solutions at 30 ± 0.5 °C. A wide range of CMP solution chemistries was employed to examine the effects of these chemistries on the environment-assisted crack growth. These included pH 7 and 10 NH $_4$ OH, pH 10 NaOH, and pH 10 KOH solutions in deionized water (DIW) without surfactants. Surfactant solutions were also tested including pH 7 and 10 NH $_4$ OH DIW solutions containing one of the 0.1 wt.% monomeric (linear) and dimeric (branched) surfactants listed in Table 1. The hydrophilic–lipophilic balance (HLB) of the surfactants was calculated by Griffin’s method [27]: $HLB = 20M_h/M$, where M_h is the molecular mass of the hydrophilic portion of the molecule, and M is the molecular mass of the whole molecule. Therefore, an HLB value of 0 corresponds to a completely hydrophobic surfactant, and a value of 20 corresponds to a completely hydrophilic surfactant. After testing, X-ray photoelectron spectroscopy (XPS) was used to determine the location of the fracture path in the thin-film stack.

The morphology of a nanoporous film surface in contact with water and the surfactant solutions, respectively, was studied by atomic force microscopy (AFM) using a Multi-mode microscope (Veeco, Santa Barbara, CA). Imaging was performed with silicon nitride cantilevers with a spring constant of 0.22 N m $^{-1}$ and a tip radius of 20 nm. Force–displacement curves were also characterized to measure the bridging force of surfactant aggregates on the nanopor-

ous organosilicate film surface. The in situ measurements in the aqueous solutions were performed in soft contact mode using an AFM liquid cell.

3. Results and discussion

We consider first the effects of electrolyte solutions on crack growth behavior and then show the effects of surfactant additions. Moisture-assisted crack growth in organosilicate films is a time-dependent mode of fracture that involves a stress-enhanced chemical reaction between strained Si–O bonds at the crack tip and reactive environmental species such as water (H $_2$ O) and hydroxide (OH $^-$) [3,16–21]. The reactions can be described by:



In basic solutions, the hydroxide ions dominate the crack tip reaction, while in acidic solutions, water molecules mediate crack growth, and hydronium ions inhibit the reaction kinetics. At intermediate pH values, both crack tip reactions occur in parallel. Hydrogen peroxide (H $_2$ O $_2$) has been shown to significantly accelerate the crack growth due to its strong affinity for electrons which weakens the Si–O crack tip bonds by reducing the electron density in the bonding orbitals [2].

To demonstrate the effects of alkali metal ions on the crack growth in nanoporous organosilicate glasses, a multilayer thin-film stack containing a nanoporous organosilicate film (Fig. 2) was tested in pH 7 and 10 NH $_4$ OH, and pH 10 NaOH and KOH solutions. Crack growth rates measured as a function of applied strain energy release rate, G , are shown in Fig. 3. In the NH $_4$ OH solutions, crack growth rates were accelerated when the pH was increased from 7 to 10, consistent with the previously reported dependence of crack growth rates on pH [3,21]. Surprisingly, however, the crack growth rates were decelerated in pH 10 NaOH and KOH solutions compared to the pH 10 NH $_4$ OH solution, and slower even than those mea-

Table 1

Polyoxyethylene alkyl ethers and dimeric surfactants selected for the crack-growth tests. Hydrocarbon and EO chain lengths, HLB, and molecular weight are listed.

Type	Name	No. of C, m	No. of EO, n	Hydrophilic–lipophilic balance, HLB	Molecular weight, M (g mol $^{-1}$)
Monomeric	C $_{10}$ E $_4$	10	4	10.5	334
	C $_{10}$ E $_6$		6	12.4	423
	C $_{10}$ E $_9$		9	14.3	555
	C $_{12}$ E $_4$	12	4	9.2	363
	C $_{12}$ E $_7$		7	12.2	495
	C $_{12}$ E $_{23}$		23	16.8	1200
	C $_{12}$ E $_{50}$	18	50	18.3	2389
	C $_{18}$ E $_{10}$		10	12.4	711
	C $_{18}$ E $_{20}$		20	15.3	1152
	C $_{18}$ E $_{100}$		100	18.8	4676
Dimeric	D-1	14	1.3	4	284
	D-2		3.5	8	381
	D-3		10	13	667
	D-4		30	17	1548



Fig. 2. Schematic illustration of a sandwiched multilayer thin-film stack.

sured in the pH 7 NH_4OH solution. For example, at pH 10 and $G = 1.7 \text{ J m}^{-2}$, the crack growth rate was decreased by about one order of magnitude by changing the cation in solution from NH_4^+ to Na^+ , and another order of magnitude from Na^+ to K^+ . The suppression in crack growth rates is even more obvious when comparing the threshold value of the applied strain energy release rate, G_{th} , below which crack growth is dormant. For the pH 10 solutions, G_{th} values increased from $\sim 1.35 \text{ J m}^{-2}$ in NH_4OH , to $\sim 1.45 \text{ J m}^{-2}$ in NaOH , and $\sim 1.62 \text{ J m}^{-2}$ in KOH . The marked effect of cation type on the crack growth rate has not been reported for organosilicate glass films. On the other hand, the interaction of reactive hydroxide anions with strained Si—O crack tip bonds has been reported [3,21].

We believe the suppression of crack growth rates is related to crack tip blunting caused by the alkali metal ions through dissolution and reprecipitation of the siloxane network of the organosilicate film and similar to that reported in bulk silicate glasses [28,29]. Alkali metal ions promote

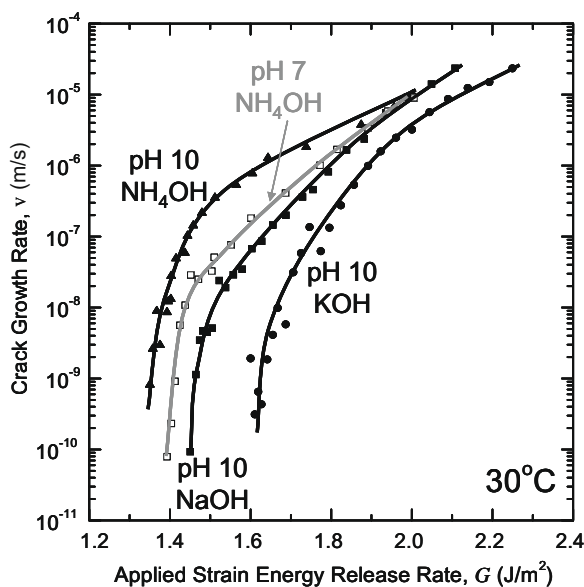


Fig. 3. Effects of pH and alkali metal ions of pH 10 solutions on the crack growth rate in a nanoporous organosilicate film as a function of applied strain energy release rate. A v - G curve for a pH 7 NH_4OH solution is shown in a grey line as a reference.

the dissolution of the Si—O—Si backbone and the dissolution rate increases in the order $\text{NH}_4\text{OH} < \text{NaOH} < \text{KOH}$ [30]. The dissolved Si—O—Si backbone in the form of silicic acid, $\text{Si}(\text{OH})_4$, reprecipitates at the crack tip because of the decreased solubility of silica in water at the crack tip due to the negative curvature of the crack tip (Fig. 4) [28,29]. The subsequent increase in the crack tip radius of curvature, ρ , results in a decrease in the crack tip stress fields which scale with $\rho^{-1/2}$ as described by the Inglis solution [31]. The reduced crack tip stress fields can be directly related to a reduction in the strain energy release rate, G , and hence a lower crack driving force and reduced crack growth velocity with increasing dissolution of the crack tip.

We now demonstrate the dramatic effects of a range of common nonionic surfactants on the crack growth behavior in selected electrolyte solutions. Polyoxyethylene alkyl ethers (Fig. 5a), $\text{CH}_3(\text{CH}_2)_{m-1}(\text{OCH}_2\text{CH}_2)_n\text{OH}$ or C_mE_n , with various hydrophobic alkyl tail lengths, m , and hydrophilic ethylene oxide (EO) head lengths, n , were selected as monomeric surfactants to systematically study the roles of the hydrophobic and hydrophilic group lengths in the crack growth rates of the nanoporous organosilicate film. Dimeric surfactants (Fig. 5b) were also tested to reveal the effect of the molecular structure of surfactants on the crack growth rates. Properties of the selected surfactants, including hydrocarbon and EO chain lengths, the HLB, and molecular weight, are listed in Table 1. The crack growth rates measured as a function of G were significantly suppressed in the presence of 0.1 wt.% C_mE_n surfactants for both the pH 7 (Fig. 6) and pH 10 (Fig. 7) NH_4OH solutions. At pH 7, C_{10}E_n surfactants significantly suppressed the crack growth and increased G_{th} values with longer hydrophilic head lengths (Fig. 6a). G_{th} increased systematically in the order 1.4 J m^{-2} without surfactant $< 1.6 \text{ J m}^{-2}$ with surfactant having four EO units $< 1.7 \text{ J m}^{-2}$ with surfactant having six EO units $< 1.9 \text{ J m}^{-2}$ with surfactant having nine EO units. C_{12}E_n surfactants, which have the longer hydrophobic tails than those of C_{10}E_n surfactants, further reduced the crack growth rates, but the hydrophilic head length dependency was less apparent (Fig. 6b). C_{18}E_n surfactants, however, had almost no effect on the crack growth

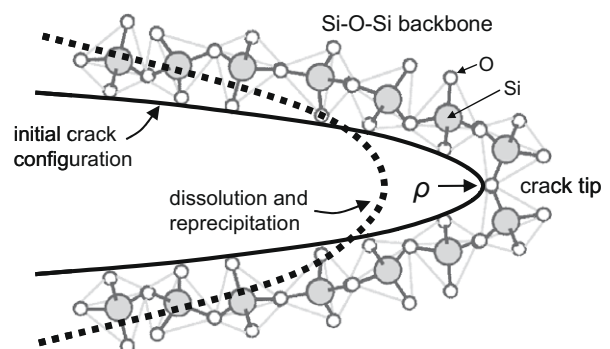


Fig. 4. Schematic illustration of crack tip blunting by dissolution and reprecipitation.

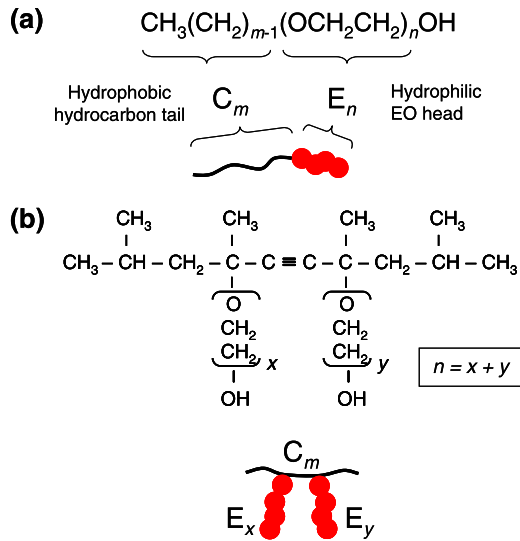


Fig. 5. Molecular structure of (a) polyoxyethylene alkyl ethers and (b) dimeric surfactants.

rates (Fig. 6c). At pH 10, the crack growth rates were reduced for the surfactants with longer hydrophobic tail lengths (Fig. 7). We note that $C_{18}E_n$ surfactant additions dramatically suppressed the crack growth (Fig. 7c). These results are in sharp contrast to the insensitivity of the crack growth to $C_{18}E_n$ surfactant additions in pH 7 NH_4OH solutions. Of these surfactants with a hydrocarbon chain length of 18, $C_{18}E_{20}$ suppressed the crack growth rates most, increasing the G_{th} value from $\sim 1.35 \text{ J m}^{-2}$ (in the pH 10 NH_4OH solution without the surfactant) to $\sim 2.1 \text{ J m}^{-2}$ (in the pH 10 NH_4OH solution with the surfactant). This value is much higher than G_{th} in air ($\sim 1.7 \text{ J m}^{-2}$), which implies the surfactant is able to suppress or even shut down crack growth. Generally even small changes in the hydrophobic hydrocarbon tail length m and hydrophilic EO head length n of C_mE_n surfactants dramatically suppressed the growth rate of cracks in nanoporous organosilicate materials. Conversely, 0.1 wt.% dimeric surfactant additions significantly accelerated the crack growth in nanoporous organosilicate films compared to the crack growth rates without surfactants as shown in Fig. 8a. For values of applied G in the range ~ 1.4 – 2.0 J m^{-2} , growth rates were found to increase by up to nearly two orders of magnitude for the solution containing the D-2 surfactant compared to the control.

The addition of nonionic surfactants therefore resulted in two opposite effects on crack growth rates. C_mE_n surfactants suppressed and dimeric surfactants accelerated crack growth rates compared to growth rates in the absence of surfactants. We consider first the accelerated crack growth in the presence of the dimeric surfactants, which may be related to their superior surface wetting and related low foaming (defoaming) properties. This leads to a decrease in the surface energy, γ_F , of the crack surfaces formed in the organosilicate film. Using chemical reaction rate models, the crack growth rate, v , can be related to γ_F [3,16,32–35]:

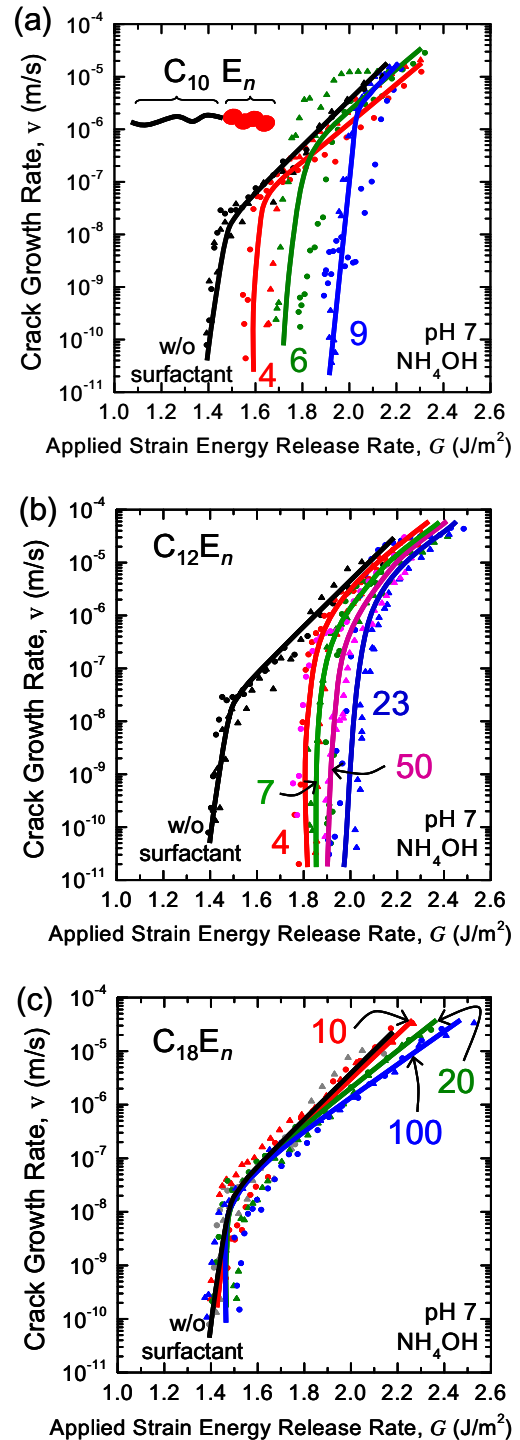


Fig. 6. Crack growth rates as a function of G , observed for pH 7 NH_4OH solutions with 0.1 wt.% of (a) $C_{10}E_n$, (b) $C_{12}E_n$ and (c) $C_{18}E_n$ surfactants, respectively.

$$v = v_0 \exp[\alpha(G - 2\gamma_F)/kT] \quad (3)$$

where v_0 is a material-dependent reference velocity, α is an activation area for the crack tip reaction and related to the slope of the v – G curve, k is the Boltzmann constant, and T is the absolute temperature. With different dimeric surfactants additions the slope α of the v – G curves was constant and equal to the slope in the absence of surfactants

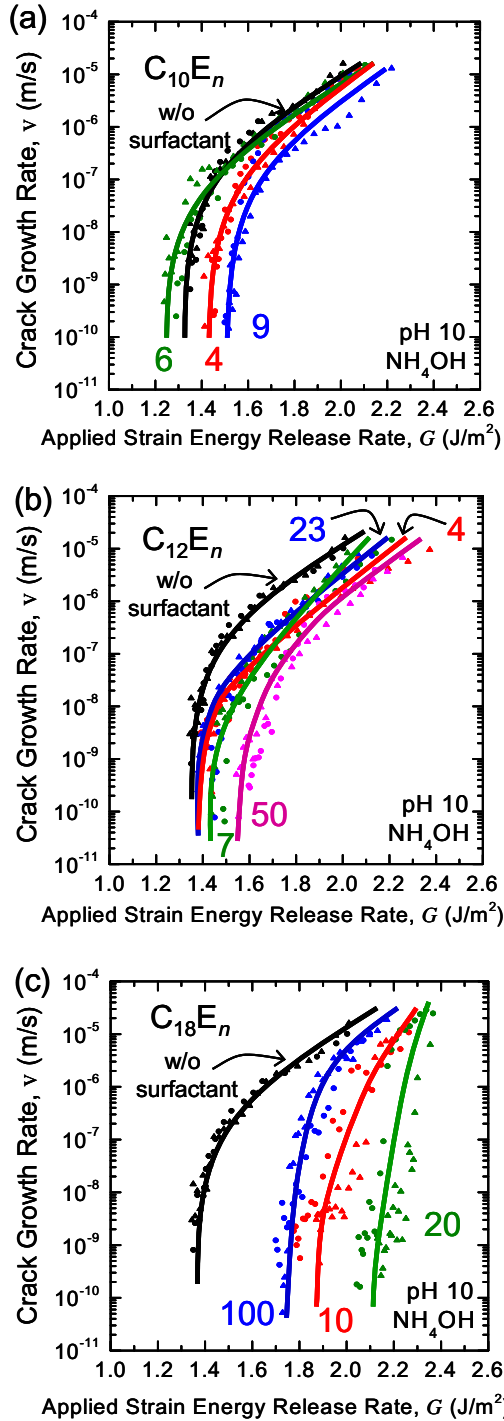


Fig. 7. Crack growth rates as a function of G , observed for pH 10 NH_4OH solutions with 0.1 wt.% of (a) C_{10}E_n , (b) C_{12}E_n and (c) C_{18}E_n surfactants, respectively.

(Fig. 8a). Therefore the ratio of the crack growth rate in the solution with surfactant, v_{L_s} , to the crack growth rate in the solution without surfactant, v_L , can be expressed as:

$$\frac{v_{L_s}}{v_L} = \exp[-2\alpha\Delta\gamma_F/kT] \quad (4)$$

where $\Delta\gamma_F$ is the change in the crack surface energy in the presence of the surfactant solution relative to the solution

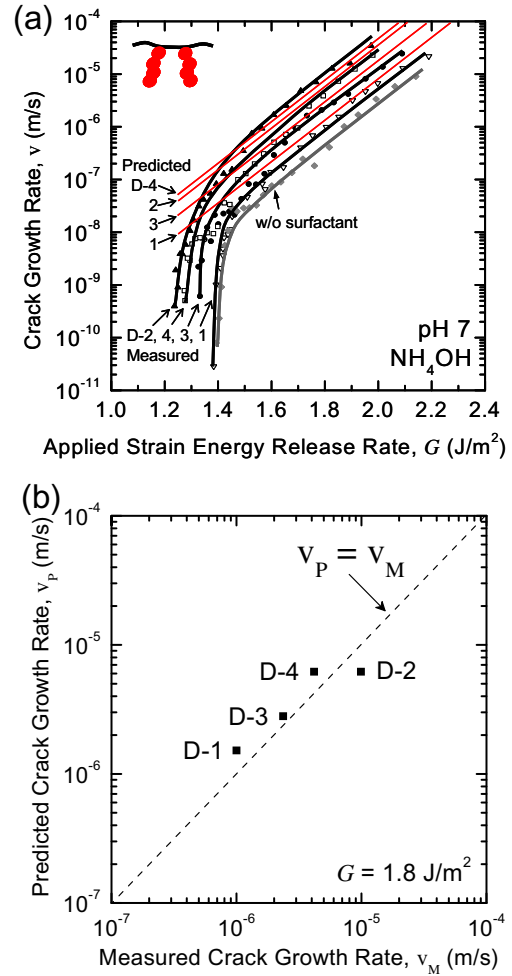


Fig. 8. Crack growth rates were significantly accelerated in pH 7 NH_4OH solutions with 0.1 wt.% dimeric surfactants as shown in (a) the v - G plot where straight lines show the predicted crack growth rates in the solutions, and (b) the predicted crack growth rates at applied $G = 1.8 \text{ J m}^{-2}$ are compared with the measured. (For interpretation of the references to colour in this figure legend, the reader is referred to the web version of this article.)

without surfactant. $\Delta\gamma_F$ can be calculated using Young's equation:

$$\Delta\gamma_F = \gamma_{F-L_s} - \gamma_{F-L} = -\gamma_{L_s-A} \cos \theta_{L_s} + \gamma_{L-A} \cos \theta_L \quad (5)$$

where γ_{F-L_s} is the surface energy of the film in contact with the surfactant solution (L_s), γ_{F-L} is the surface energy of the film in contact with the solution without surfactant (L), γ_{L_s-A} is the surface tension of the L_s -air interface, γ_{L-A} is the surface tension of the L -air interface, and θ_{L_s} and θ_L are the contact angles of L_s and L with the nanoporous film surface, respectively. The measured values for θ_L and γ_{L-A} for the pH 7 NH_4OH solution without surfactant are 100° and 72 mN m^{-1} , respectively. The values of θ_{L_s} and γ_{L_s-A} are 53° and 32 mN m^{-1} for the pH 7 NH_4OH solution with 0.1 wt.% of the D-1 surfactant, 21° and 33 mN m^{-1} for the D-2 surfactant solution, 50° and 42 mN m^{-1} for the D-3 surfactant solution, and 47° and 51 mN m^{-1} for the D-4 surfactant solution, respectively. Using Eqs. (4) and (5), the

predicted crack growth rates are shown in Fig. 8 and were found to be in good agreement with the measured growth rates. This suggests that the accelerated crack growth observed is related to a decrease of the crack surface energy formed in the presence of the dimeric surfactants.

Unlike in the dimeric surfactant solutions, crack growth rates were significantly suppressed in the C_mE_n -containing solutions. The C_mE_n surfactants are not known to be effective wetting agents like the dimeric surfactants, and contact angle measurements revealed that they were also not as effective at lowering the surface energy of the organosilicate films. For example, the contact angle θ_{LS} for the $C_{10}E_9$ surfactant in the pH 7 NH_4OH solution was 60° . We therefore do not expect them to accelerate growth rates. In fact, C_mE_n surfactants further suppressed the crack growth rates compared to the solutions without them as shown in Figs. 6 and 7. We now discuss energy dissipation processes related to crack bridging effects from two possible sources that explain the suppression of crack growth rates. These processes are expected to dominate any possible acceleration of the crack growth related to the small changes in crack surface energy. The first mechanism is the formation of molecular bridging from micelles and bilayer assemblies of surfactants. As shown in Fig. 1b, C_mE_n surfactants may form micelles and bilayer assemblies of surfactants that bridge two crack surfaces in the wake of the crack. The hydrophobic methyl groups on both crack surfaces may participate in the formation of the bridging micelles via the hydrophobic interaction between the methyl groups and the alkyl groups of the surfactant molecules resulting in the bridging contribution. The hydrogen bonding between the polar EO groups and hydrophilic hydroxyl groups on the surfaces may also contribute to the formation of the bridging micelles and bilayers. We note that the structure and connectivity of the bridging surfactant aggregates is expected to be sensitive to surfactant concentration, hydrophilic head and hydrophobic tail lengths, pH and the type of electrolyte. We found in fact that surfactant solutions with 0.01 wt.% $C_{18}E_{20}$ significantly suppressed the crack growth, whereas a higher concentration of 0.1 wt.% did not affect the crack growth rate (Fig. 9). Reported phase diagrams for this surfactant suggest a dramatic change from cylindrical or bilayer structures for the 0.01 wt.%, while spherical micelles form at 0.1 wt.% surfactant [36]. It appears that the spherical micelles do not form effective crack bridging elements while the cylindrical or bilayer structures bridge the crack surfaces and consequently suppress the crack growth rate.

The second possible mechanism for the bridging is nanobubble formation and cavitation enhanced by surfactants. When a hydrophobic surface comes into contact with water, nanobubbles can be formed on the surface and the direct evidence of nanobubble formation has been revealed with the help of AFM imaging [37,38]. In the case of two parallel hydrophobic surfaces approaching each other in water, nanobubbles on each surface can coalesce, leading to an attractive Laplace pressure by the cavity bridging

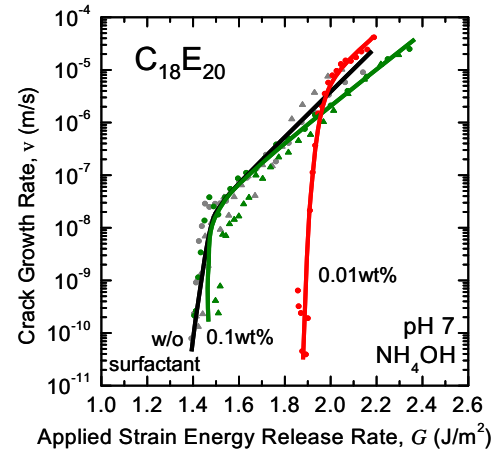


Fig. 9. The effect of surfactant concentration on the crack growth rate. The surfactant solution with 0.01 wt.% $C_{18}E_{20}$ significantly suppressed the crack growth, whereas 0.1 wt.% $C_{18}E_{20}$ did not affect the crack growth rate noticeably.

the two surfaces [38,39]. The nanobubble and subsequent cavity formation would be enhanced and stabilized in the presence of high foaming surfactants such as polyoxyethylene alkyl ethers (C_mE_n). Therefore we can envision a crack bridging phenomenon by surfactant-enhanced nanobubble cavitation in four steps as shown in Fig. 10a–d.

In both cases, the crack driving force at the crack tip, G_{tip} , will be decreased by the bridging contribution, $G_{bridging}$, as follows:

$$G_{tip} = G_{applied} - G_{bridging} \quad (6)$$

where $G_{applied}$ is the applied strain energy release rate. No matter what mechanism dominates the bridging effect, the steady-state bridging contribution $G_{bridging}$ may be approximated using a stress–separation curve, σ – δ , with

$$G_{bridging} = \sigma_o \delta_o \int_0^1 \chi(\varepsilon) d\varepsilon \quad (7)$$

where σ_o is a maximum bridging stress, δ_o is a maximum bridging separation across the crack surfaces, ε is the bridging strain, $d\varepsilon/d\delta$, and χ describes the shape of the σ – δ curve [40,41]. One of methods to directly measure σ_o and δ_o is pulling the surfactant aggregates with an AFM probe. As shown in the AFM topography image of interface between a nanoporous film surface and aqueous pH 10 NH_4OH without surfactant (inset, Fig. 11a), the interface is featureless and flat. However, in the presence of 0.1 wt.% $C_{18}E_{20}$ surfactant in the solution, the surfactant aggregates self-assemble on the nanoporous film surface (Fig. 11a). When we pushed and pulled the surfactant aggregates with an AFM tip, a significant bridging force was detected as shown in the force–displacement plot (Fig. 11b). Surprisingly the bridging was sustained for a very long range of displacement of more than 350 nm. This implies that surfactant molecules can bridge two crack surfaces in the nanoporous organosilicate film from very near the crack tip where elastic crack opening is on the molecular scale to tens of micrometers behind the

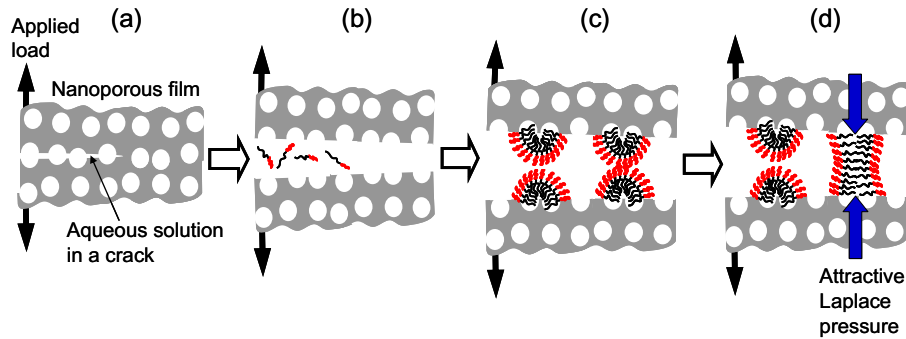


Fig. 10. A crack bridging phenomenon by surfactant-enhanced nanobubble cavitation consisting of the following four steps. (a) Crack propagates in a hydrophobic nanoporous organosilicate film and nanobubbles nucleate instantly on crack surfaces in contact with an aqueous solution. (b) Surfactants are attracted to air–water nanobubble interfaces. (c) Surfactants adsorb on nanobubbles and facilitate the growth of nanobubbles. (d) Finally, nanobubbles coalesce and the resulting cavity generates an attractive Laplace pressure at large range.

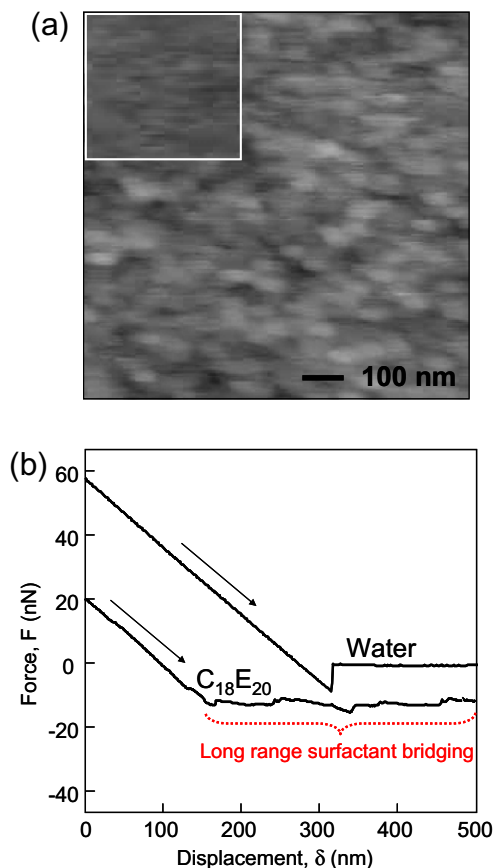


Fig. 11. The in situ AFM characterizations of the surfactant self-assemblies and their bridging force measured in the aqueous solutions. (a) An AFM image of $C_{18}E_{20}$ aggregates adsorbed to the interface between a nanoporous film surface and NH_4OH pH 10 water containing 0.1 wt.% $C_{18}E_{20}$ surfactant. An inset shows an AFM image of interface between a nanoporous film surface and NH_4OH pH 10 water without surfactant. (b) AFM force–displacement curves measured between a nanoporous film surface and aqueous pH 10 NH_4OH with and without 0.1 wt.% $C_{18}E_{20}$ surfactant, respectively. Arrows indicate the direction of AFM probe retraction. Significant long-range surfactant bridging was observed for the $C_{18}E_{20}$ solution.

crack tip where elastic crack opening is of the order of hundreds of nanometers. The resulting σ_o and δ_o for the $C_{18}E_{20}$ surfactant aggregates are approximately 2.65 pN nm^{-2} and

350 nm , respectively. The maximum bridging force, $F_{\max} \sim 13.3 \text{ nN}$, and bridging area, $A \sim \pi \times (C \times r)^2 \sim 5027 \text{ nm}^2$, was used to calculate $\sigma_o = F_{\max}/A$, where C is a constant to determine the areal coverage and estimated to be ~ 2 , and r is the radius of the AFM tip. The value of δ_o is estimated from Fig. 11b, but is consistent with previously reported data [42]. Assuming the shape function χ is rectilinear, the calculated G_{bridging} value using Eq. (7) is $\sim 0.93 \text{ J m}^{-2}$ and this is reasonably close to the $\Delta G_{th} \sim 0.75 \text{ J m}^{-2}$ for the $C_{18}E_{20}$ surfactant solution observed in Fig. 7c. This clearly implies that surfactant bridging can result in the significant suppression of the crack growth rates.

We note that aqueous solutions containing organic species may diffuse into strongly hydrophobic nanoporous organosilicate glass films [22]. The penetrating aqueous solution can change the surface stress of the film, resulting in expansion and contraction associated with elastic strains in the film [4]. In the case of expansion of the film sandwiched between two Si substrates, the relaxation would create a compressive elastic stress in the film, and consequently reduce the crack driving force at the crack tip G_{tip} , leading to suppression of crack growth rates near the threshold G_{th} [4]. This might be a possible mechanism for the suppression of the crack growth rates observed in Figs. 6 and 7. However, the rate of diffusion of the solutions into the films is sufficiently slow that the effect is important only at relatively low crack growth rates where the solution has time to diffuse into the layer on either side of the crack. In the case of high growth rates, the solution simply does not have sufficient time to diffuse into the material and there is no effect on the measured crack growth rates. On the contrary, the suppression of the crack growth by the addition of the surfactants occurred even at relatively high crack growth rates $v > 10^{-7} \text{ m s}^{-1}$ as shown in Figs. 6 and 7. Moreover, the most significant crack suppression effect was observed for $C_{18}E_n$ surfactants in pH 10 (Fig. 7c), which have lower diffusivities in the nanoporous film compared to those of $C_{10}E_n$ and $C_{12}E_n$ surfactants [43]. Therefore, it is unlikely that the compressive stress at the crack tip induced by the diffusion of the aqueous solutions mainly causes the suppression of the crack growth rates observed in this study.

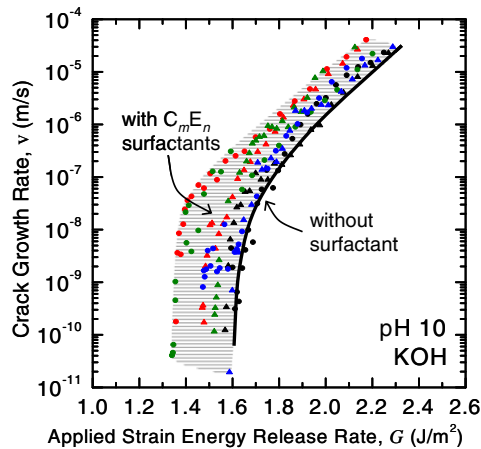


Fig. 12. Crack growth rates as a function of G , observed for pH 10 KOH solutions. A solid line represents a v - G curve for a pH 10 KOH solution without surfactant. The hatched band includes all v - G curves for pH 10 KOH solutions with 0.1 wt.% C_mE_n surfactants.

The 0.1 wt.% C_mE_n surfactant additions in pH 10 KOH solutions did not result in the suppression of the crack growth, but rather increased crack growth rates compared to the solution without surfactant (Fig. 12). We believe this is associated with the immobilized EO chains of the surfactants by the complexation with potassium ions and the subsequent decrease in free potassium ion concentration leading to the mitigation of both bridging and crack tip blunting effects. Alkali metal ions such as K^+ and Na^+ can be trapped in the EO chains of the surfactants by their complexation with the EO chains [44–47]. The EO chain can adopt a helix and trap alkali metal ions in the molecular cavity by electrostatic bonding between the metal ion and the oxygen in EO [44]. The complexed surfactant molecules may not contribute to the bridging of self-assembly due to their immobilized EO chains. Moreover, the concentration of the potassium ion available for the crack tip blunting would be decreased by the complexation, resulting in the accelerated crack growth compared to the solution without surfactant as shown in Fig. 12.

4. Conclusions

This study shows that small changes in electrolyte chemistry and surfactant additions can have dramatic effects on crack growth rates in nanoporous organosilicate thin films. Crack growth rates were sensitive to the type of electrolyte and decreased in the presence of electrolytes that caused crack tip blunting. Growth rates were also sensitive to non-ionic surfactant additions where molecular structure and weight were demonstrated to be important variables. C_mE_n surfactants significantly retarded crack growth rates, whereas dimeric surfactants accelerated the crack growth process. The dimeric surfactants were shown to accelerate growth rates by lowering the surface energy of the fracture surface. The suppression of crack growth rates in C_mE_n surfactant solutions was attributed to crack bridging result-

ing from the formation of molecular assemblies of surfactants, or the formation of nanobubbles and their cavitation, across crack surfaces. Surfactant self-assembly and resulting molecular bridging were characterized by in situ AFM and used to quantify the molecular bridging observed.

Acknowledgments

The authors acknowledge assistance with AFM tests by Rachel Elizabeth Maire. T.K. was supported by JSR Micro, Inc. The work was supported by the Director, Office of Energy Research, Office of Basic Energy Sciences, Materials Sciences Division of the US Department of Energy, under Contract No. DE-FG02-07ER46391.

References

- [1] International technology roadmap for semiconductors. 2007 ed. Interconnect: Semiconductor Industry Association; 2007.
- [2] Guyer EP, Dauskardt RH. *Nat Mater* 2004;3:53.
- [3] Guyer EP, Dauskardt RH. *J Mater Res* 2005;20:680.
- [4] Guyer EP, Patz M, Dauskardt RH. *J Mater Res* 2006;21:882.
- [5] Ro HW, Char K, Jeon E-C, Kim H-J, Kwon D, Lee H-J, et al. *Adv Mater* 2007;19:705.
- [6] Cheetham AK, Ferey G, Loiseau T. *Angew Chem Int Ed* 1999;38:3268.
- [7] Desai TA, Hansford DJ, Leoni L, Essenpreis M, Ferrari M. *Biosens Bioelectron* 2000;15:453.
- [8] Chen W-C, Lee L-H, Chen B-F, Yen C-T. *J Mater Chem* 2002;12:3644.
- [9] Yang P, Wirnsberger G, Huang HC, Cordero SR, McGehee MD, Scott B, et al. *Science* 2000;21:465.
- [10] Coakley KM, Liu Y, McGehee MD, Frindell KL, Stucky GD. *Adv Funct Mater* 2003;13:301.
- [11] Paik J-M, Park H, Joo Y-C, Park K-C. *J Appl Phys* 2005;97:104513.
- [12] Ring TA, Feeney P, Boldridge D, Kasthurirangan J, Li S, Dirksen JA. *J Electrochem Soc* 2007;154:H239.
- [13] Yuan C, Driel WDV, Silfhout Rv, Sluis Ovd, Engelen RAB, Ernst LJ, et al. *Microelectr Reliab* 2006;46:1679.
- [14] Guyer EP, Dauskardt RH. *IEEE International Interconnect Technology Conference Proceedings*; 2003. p. 89.
- [15] Guyer EP, Dauskardt RH. *IEEE International Interconnect Technology Conference Proceedings*; 2004. p. 236.
- [16] Wiederhorn SM. *J Am Ceram Soc* 1967;50:407.
- [17] Lawn BR. *Mater Sci Eng* 1973;13:277.
- [18] Michalske TA, Freiman SW. *Nature* 1982;295:511.
- [19] Michalske TA, Bunker BC. *J Appl Phys* 1984;56:2686.
- [20] Cook RF, Liniger EG. *J Electrochem Soc* 1999;146:4439.
- [21] Vlassak JJ, Lin Y, Tsui TY. *Mater Sci Eng* 2005;39:159.
- [22] Guyer EP, Gantz J, Dauskardt RH. *J Mater Res* 2007;22:710.
- [23] Chen W, Yen C. *J Vac Sci Technol B* 2000;18:201.
- [24] Lee J, Park Y, Yoon B, Han Y, Hah S, Moon J. *J Electrochem Soc* 2002;149:G477.
- [25] Lane MW, Snodgrass JM, Dauskardt RH. *Microelectron Reliab* 2001;41:1615.
- [26] Hohlfelder RJ, Maidenberg DA, Dauskardt RH, Wei Y, Hutchinson JW. *J Mater Res* 2001;16:243.
- [27] Griffin WC. *J Soc Cosmet Chem* 1954;5:259.
- [28] Ito S, Tomozawa M. *J Am Ceram Soc* 1982;65:368.
- [29] Tomozawa M. *Annu Rev Mater Sci* 1996;26:43.
- [30] Wijnen PWJG, Beelen TPM, Haan JWD, Rummens CPJ, Ven LJMvd, Santen RAV. *J Non-Cryst Solids* 1989;109:85.
- [31] Inglis CE. *Trans Inst Naval Archit* 1913;55:219.

- [32] Lawn BR. *J Mater Sci* 1975;10:469.
- [33] Lawn BR. *Fracture of brittle solids*. Cambridge: Cambridge University Press; 1993.
- [34] Cook RF, Liniger EG. *J Am Ceram Soc* 1993;76:1096.
- [35] Cook RF. *Mater Sci Eng A* 1999;260:29.
- [36] Mitchell DJ, Tiddy GJT, Waring L, Bostock T, McDonald MP. *J Chem Soc: Faraday Trans 1* 1983;79:975.
- [37] Tyrrell JWG, Attard P. *Phys Rev Lett* 2001;87:176104.
- [38] Ishida N, Sakamoto M, Miyahara M, Higashitani K. *Langmuir* 2000;16:5681.
- [39] Meyer EE, Rosenberg KJ, Israelachvili J. *Proc Natl Acad Sci* 2006;103:15739.
- [40] Bao G, Suo Z. *Appl Mech Rev* 1992;45:355.
- [41] Maidenberg DA, Volksen W, Miller RD, Dauskardt RH. *Nat Mater* 2004;3:464.
- [42] Butt H, Cappella B, Kappl M. *Surf Sci Rep* 2005;59:1.
- [43] Kim T, Mackie K, Zhong Q, Peterson M, Konno T, Dauskardt RH. *Nano Lett* 2009;9:2427.
- [44] Okada T. *Analyst* 1993;118:959.
- [45] Desmazières B, Portet F, Desbène P-L. *Chromatographia* 1993;36:307.
- [46] Parees DM, Hanton SD, Clark PAC, Willcox DA. *J Am Soc Mass Spectrom* 1998;9:282.
- [47] Cheng H, Clark PAC, Hanton SD, Kung P. *J Phys Chem A* 2000;104:2641.